Journal of Physics:
Conference Series

PAPER • OPEN ACCESS

Prediction and analysis of radiated noise from a small underwater vehicle

To cite this article: Fan Xu *et al* 2026 *J. Phys.: Conf. Ser.* **3170** 012006

Prediction and analysis of radiated noise from a small underwater vehicle

Fan Xu[1], Yun Zhao[2], Yu Yao[1], Xiangyu You[1], Hefeng Zhou[2*]

[1]School of Hydraulic and Ocean Engineering, Changsha University of Science and Technology, Changsha 410114, China
[2]College of Meteorology and Oceanography, National University of Defense Technology, Changsha 410073, China

[*]Corresponding author's e-mail: Zhouhefeng@nudt.edu.cn

Abstract. Small underwater vehicles are widely used in reconnaissance, infiltration, and special underwater missions due to their compact size, low noise signature, and high maneuverability. However, during typical operating conditions, vibrations induced by internal components such as electric motors and propulsion systems can be transmitted through the structure and radiate acoustic noise into the surrounding water, which compromises the vehicle's acoustic stealth and increases the risk of detection by passive sonar. In this study, a small frogman carrier is taken as the research object, and a coupled acoustic–structure interaction (ASI) finite element model is developed using COMSOL Multiphysics. The model simulates the vibroacoustic behavior of the carrier under typical excitation conditions to predict its radiated noise characteristics. Through the analysis of structure-borne vibration responses and sound pressure field distributions, the frequency spectrum, spatial directivity, and dominant source mechanisms of the radiated noise are investigated. The results provide theoretical insights and design references for low-noise design, detection risk assessment, and acoustic stealth optimization of small underwater vehicles.

1. Introduction

With the increasing diversification of maritime missions and the growing demand for stealth, small underwater vehicles—such as diver delivery vehicles (DDVs) and unmanned submersibles—have been widely deployed in reconnaissance, penetration operations, special warfare, and underwater engineering tasks. These vehicles are typically characterized by compact size, lightweight structure, high maneuverability, and strong environmental adaptability [1–2]. However, the radiated noise generated during operation not only undermines their stealth performance but also significantly increases the probability of detection by acoustic sensors, active sonar, or passive hydrophone arrays. Therefore, the analysis and predictive modeling of their acoustic signatures are of great theoretical and engineering importance.

The primary sources of radiated noise in small underwater vehicles include the electric motor, propulsion system, structural vibrations, internal fluid disturbances, and cavity resonances. These acoustic sources couple with the surrounding water medium through the vehicle hull, thereby forming a complex underwater radiated sound field [3]. In particular, in shallow water and reef environments, low-frequency noise is prone to reflection, scattering, and interference, which distorts the sound propagation paths and poses challenges to conventional target detection and classification methods. Consequently, investigating the radiated noise characteristics and underlying mechanisms of such vehicles is essential for optimizing design, enhancing underwater platform stealth, and supporting the development of anti-diver detection systems.

In recent years, with advances in multiphysics simulation platforms, finite element–based vibro-acoustic coupling analysis has become a crucial technique for studying underwater structural acoustic radiation [4]. This method enables the coupled solution of structural vibrations and the surrounding acoustic field, thereby accurately capturing the relationship between motor-induced structural responses and the distribution of underwater sound pressure fields. In particular, platforms such as COMSOL Multiphysics provide efficient acoustic–structural coupling modules, supporting accurate geometric modeling, complex boundary conditions, and frequency-domain analyses.

In this study, a small diver delivery vehicle is selected as the research object. A fully coupled structural–acoustic finite element model is developed to numerically predict and analyze its radiated noise characteristics under typical operating conditions. By simulating the structural vibration responses of the hull under motor excitation and the resulting underwater acoustic field distribution, the study identifies dominant noise source locations, spectral characteristics, and radiation directivity. The findings provide theoretical support for subsequent noise control design and target detection countermeasures.

2. Acoustic fundamentals and simulation environment

2.1. Basic assumptions

The vibro-acoustic finite element analysis assumes the fluid medium to be ideal, and the following approximation conditions must be satisfied [5]:

a. The fluid has no viscosity, and no energy dissipation occurs during acoustic wave propagation.

b. The fluid is macroscopically stationary, i.e., its initial velocity is zero. The fluid is homogeneous, with static pressure and density taken as constants.

c. The fluid motion during acoustic wave propagation is adiabatic.

d. The acoustic waves are assumed to be of small amplitude.

2.2. COMSOL simulation environment

COMSOL Multiphysics is a powerful finite element simulation software with multiphysics coupling capabilities, widely applied in structural mechanics, acoustics, fluid dynamics, and electromagnetics. In this study, the Structural Mechanics and Acoustics modules of COMSOL are employed, using the "Acoustic–Structure Interaction" interface to model and analyze the radiated noise of a small underwater vehicle in the frequency domain [6]. Figure 1 illustrates the main computational workflow in COMSOL simulations. This workflow is adopted as the basis for the prediction and analysis of radiated noise in small underwater vehicles presented in this paper.

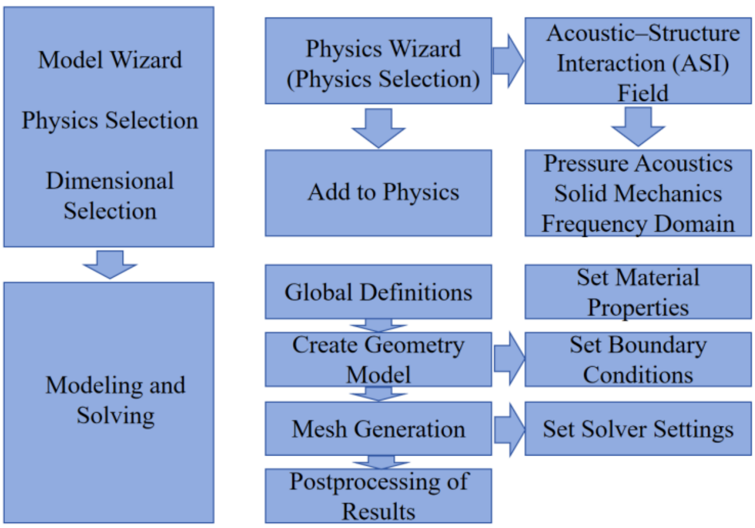

Figure 1. Simulation flowchart of acoustic–structure coupling.

2.3. Governing equations

In the frequency domain, the elastic vibrations of the solid structure and the acoustic wave propagation in the surrounding water exchange energy and momentum through the coupled interface. The governing equations consist of the structural mechanics equation and the Helmholtz equation for acoustic wave propagation.

1) Solid Structure Domain (Small Underwater Vehicle)

In the frequency domain, the solid structure is governed by the linear elastic dynamic equation:

$$-\omega^2\rho_s u+\nabla\cdot\sigma=f \tag{1}$$

where ω is the density of the solid, u is the displacement vector, σ denotes the stress tensor, and f represents the external excitation force applied to the structure.

The stress and strain are governed by the linear elastic constitutive relation:

$$\sigma=C:\varepsilon,\ \ \varepsilon=\frac{1}{2}(\nabla u+\nabla u^T) \tag{2}$$

2) Fluid Acoustic Domain (Water Medium)

The propagation of acoustic waves in the water medium can be described by the Helmholtz equation:

$$\nabla^2 p+k^2=0 \tag{3}$$

where p denotes the acoustic pressure, and k=ω/c is the acoustic wavenumber, with ω being the angular frequency and c the speed of sound in water.

3) Fluid–Structure Coupling Boundary Conditions

At the interface between the solid and the fluid (i.e., the coupling boundary), the following two conditions must be satisfied:

Continuity of normal velocity:

$$-i\omega u\cdot n=\frac{1}{\rho_f\omega}\nabla p\cdot n \tag{4}$$

Equilibrium of normal stress (pressure):

$$\sigma\cdot n=-pn \tag{5}$$

where n is the unit normal vector at the interface, and p is the acoustic pressure in the fluid.

3. Research object and computational setup

3.1. Physical model

At present, several diver delivery vehicles (DDVs) are well known internationally. Among them is the DPD series developed by STIDD Systems in the United States [7], as shown in Figure 2. The DPD series is primarily intended for military applications and is characterized by strong payload capacity.

Figure 2. DPD of STIDD from the US.

Based on the measured structural data of a specific DPD model, a solid model of the small diver delivery vehicle was constructed in the COMSOL environment. The resulting three-dimensional model of the vehicle is shown in Figure 3.

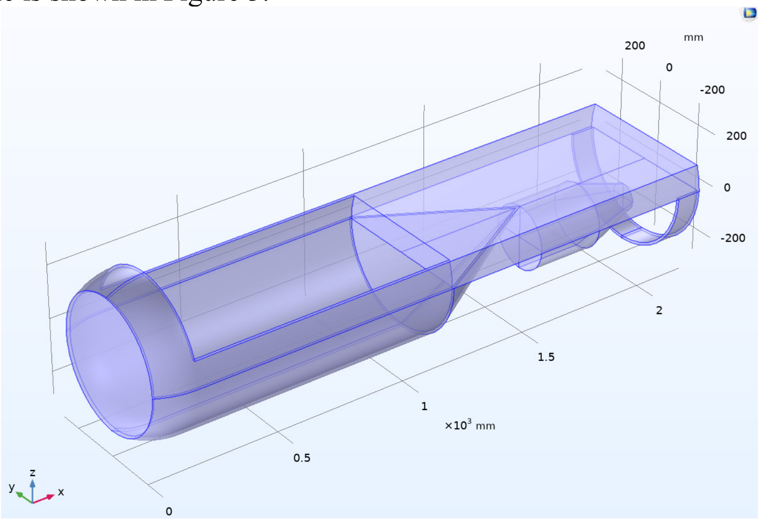

Figure 3. Model diagram of the small diver propulsion device.

3.2. Mesh generation

A three-dimensional fluid–structure interaction (FSI) model was constructed in the COMSOL environment. The total length of the vehicle model is L=2.2 m, and the maximum diameter of the cylindrical shell is D=0.57 m. The hull and local structural components are made of aluminum alloy, with material properties defined as: density ρ=2700 kg/m^3, Young's modulus E=6.9 e^{10} N/m^2, and Poisson's ratio μ=0.33.

The surrounding fluid medium is seawater, with density ρ_0=1025 kg/m^3 and sound speed c_0=1500 *m/s*. The computational domain is defined as a water region of 4 m×3 m×3 m, with a perfectly matched layer (PML) applied at the outer boundaries to eliminate spurious reflections. The geometric model is illustrated in Figure 4.

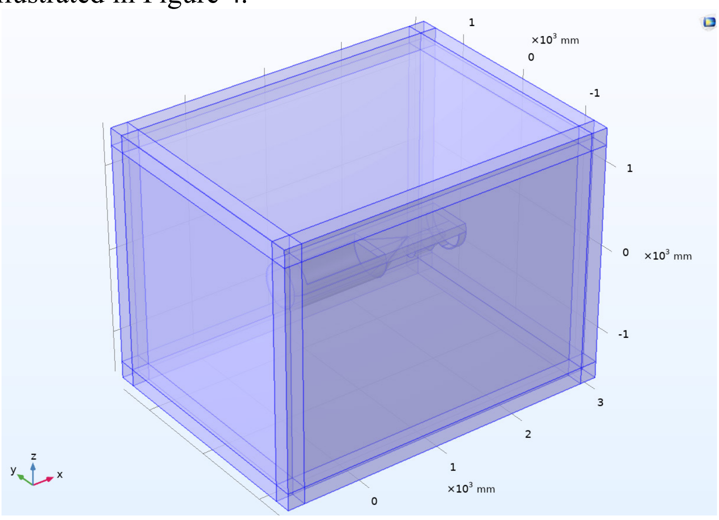

Figure 4. Coupled acoustic–structural model of the small DPD.

The model shown in Figure 4 was discretized using a tetrahedral mesh, and the finite element model of the small underwater vehicle was established as illustrated in Figure 5. The model contains approximately 30, 000 mesh vertices and about 70, 000 tetrahedral elements.

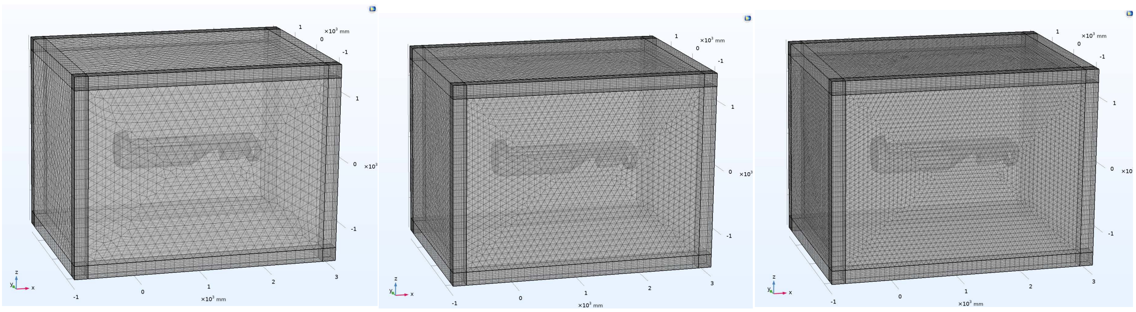

(a) Coarse Mesh (b) Medium Mesh (c) Fine Mesh

Figure 5. Acoustic–structure coupled finite element model of the small DPD.

Table 1. The mesh sensitivity analysis of the small underwater vehicle.

Mesh Level	Number of Elements	100 Hz Lp (dB)	1000 Hz Lp (dB)	2000 Hz Lp (dB)
Coarse Mesh	238724	66.058	77.858	69.699
Medium Mesh	605371	66.058	77.898	69.639
Fine Mesh	1290298	66.058	77.898	69.639

To ensure computational accuracy and reliability, a mesh sensitivity analysis was performed at three representative frequencies: 100 Hz, 1000 Hz, and 2000 Hz. The results for different mesh densities are summarized in Table 1. As the mesh was refined from coarse (238, 724 elements) to medium (605, 371 elements) and fine (1, 290, 298 elements), the far-field sound pressure level (SPL) results remained largely consistent. At 100 Hz, the results from all three mesh densities were identical. At 1000 Hz and 2000 Hz, the medium and fine mesh results were completely consistent, while the differences compared to the coarse mesh were only 0.04 dB and 0.06 dB, respectively, both far below 1%. These findings indicate that the model has achieved numerical convergence at medium or higher mesh densities. Considering both computational accuracy and resource consumption, all subsequent simulations in this study were conducted using the medium-density mesh to balance convergence and computational efficiency.

3.3. Validation of method effectiveness

To verify the reliability of the numerical method, a steel elastic spherical shell with a radius of 0.2 m, a thickness of 0.1 m, Young's modulus of 205 GPa, Poisson's ratio of 0.28, and a density of 7850 kg/m³ was used as a benchmark example. A base acceleration excitation was applied along the z-axis, and the variation of the sound pressure level at a distance of 50 m was calculated over the frequency range of 100–3000 Hz.

Table 2. SPL of the Sphere at Different Frequencies.

	100Hz Lp (dB)	300Hz Lp (dB)	500Hz Lp (dB)	600Hz Lp(dB)	1200Hz Lp (dB)	1800Hz Lp (dB)	2000Hz Lp (dB)	2500Hz Lp (dB)	3000Hz Lp (dB)
Analytical Solution	43.510	46.188	49.012	69.699	55.036	56.476	56.687	57.159	59.995
COMSOL Solution	43.550	46.250	49.050	69.639	55.000	56.470	56.680	57.160	60.000

As shown in Table 2, The comparative results indicate that the analytical solution exhibits a linear increase in the low-frequency range (100–500 Hz), followed by a slower growth and plateau in the mid-frequency range (600–1800 Hz), and then a significant rise again in the high-frequency range (2000–3000 Hz), reaching 59.9 dB at 3000 Hz. Comparison with the COMSOL simulation shows that the two results share essentially the same variation trends across all frequency ranges, with discrepancies generally below 0.2 dB and a root mean square error of approximately 0.07 dB. This demonstrates that COMSOL can accurately capture the base-excitation response of the elastic spherical shell and the associated acoustic–structure coupling effects, thereby validating its accuracy and reliability in modeling underwater acoustic radiation of elastic bodies.

3.4. Computational setup

To simulate the structural vibration-induced radiated noise of a small diver delivery vehicle during motor operation, the motion boundary similarity method was employed. The excitation was applied in the form of vibration acceleration at the motor mounting base located at the bottom of the vehicle. This approach allows for the equivalent simulation of typical vibration characteristics induced by mechanical equipment without modeling the complex internal structure of the motor. An acceleration of $a = 1\ \mathrm{m/m^2}$ was applied at the motor location along the z-axis. The main considerations for this setup are as follows: First, the focus of this study is on investigating the variation of acoustic radiation characteristics with frequency and environmental conditions, rather than reproducing the exact vibration spectrum of a specific motor. Second, the constant acceleration excitation offers good controllability and repeatability, facilitating the establishment of a unified computational benchmark and minimizing the introduction of excessive uncertainties. This simplified approach does not capture the multi-harmonic characteristics of the motor during actual operation, and therefore, the amplitude and location of resonance peaks may deviate from real conditions. In future work, more detailed modeling of motor excitation will be conducted by incorporating measured vibration spectra or harmonic superposition methods, aiming to improve the accuracy and engineering applicability of the simulation results. The calculation frequency range is 10–800 Hz with an analysis step of 2 Hz, while for the 100–3000 Hz range, the analysis step is 100 Hz.

4. Results and discussion

Based on the numerical prediction model of the radiated noise of the small underwater vehicle, frequency-domain analysis is employed to conduct underwater radiated noise simulations. First, the motion boundary similarity method is applied, where the excitation load is introduced in the form of vibration acceleration levels [8]. The source level is taken as the characteristic parameter to represent the underwater radiated noise. Furthermore, sound pressure evaluation points are arranged along a circular path with a radius of 50 m, as illustrated in Figure 6. The calculation frequency range is 10–800 Hz with an analysis step of 2 Hz, while for the 100–3000 Hz range, the analysis step is 100 Hz.

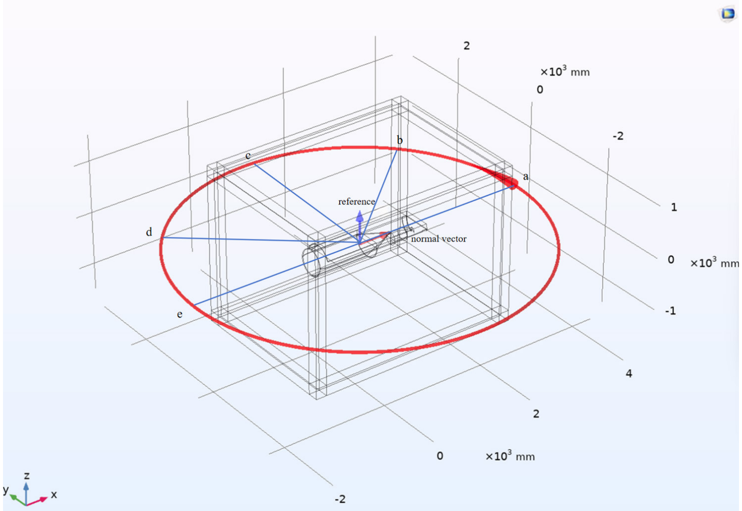

Figure 6. Computational plane for acoustic radiation of the small underwater vehicle.

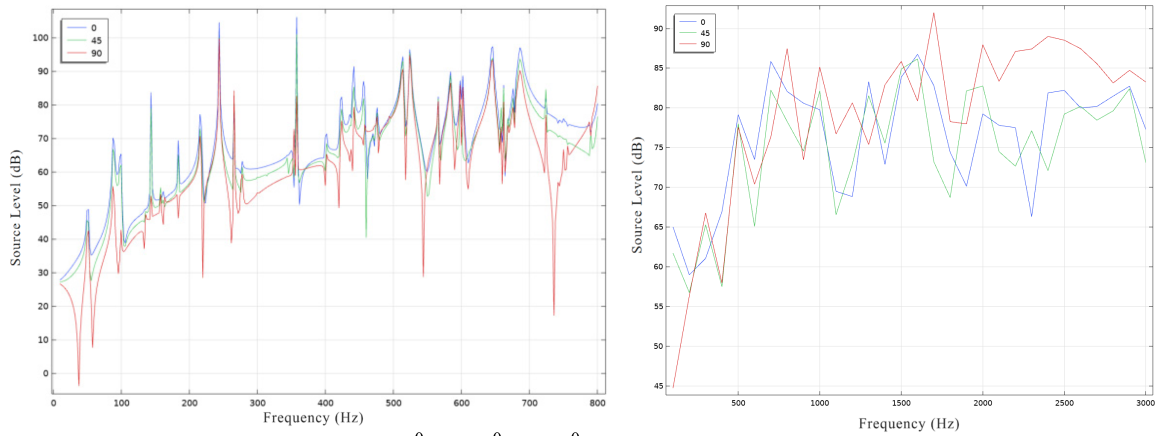

(a) θ=0^0, θ=45^0, θ=90^0 linear spectrum level

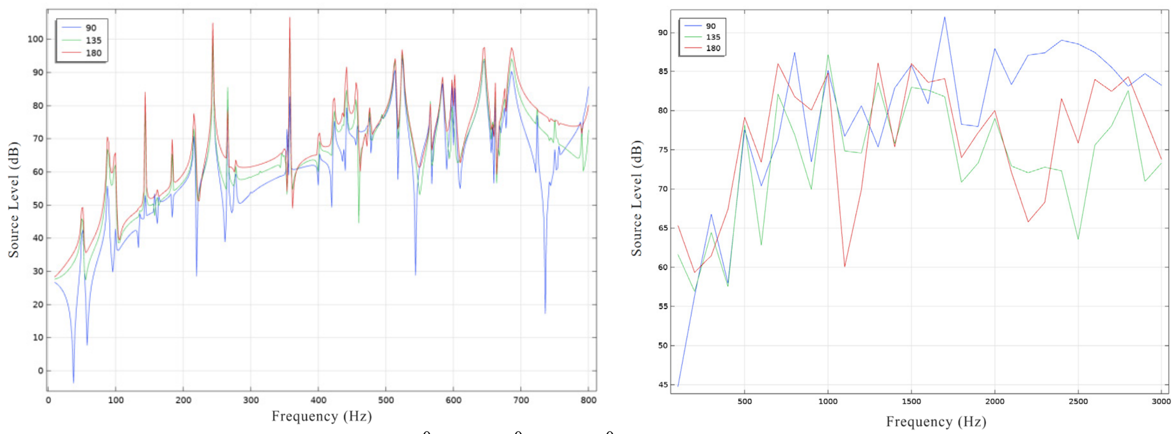

(b) θ=90^0, θ=135^0, θ=180^0 linear spectrum level

Figure 7. Numerical simulation results of acoustic radiation from the small underwater vehicle at typical directivity angles.

From the above figure 7, the frequency response analysis of the far-field sound pressure level (SPL) of the small underwater vehicle under base acceleration excitation was carried out. Five evaluation points corresponding to azimuth angles of 0°, 45°, 90°, 135°, and 180° in the horizontal plane were selected for comparison. The results indicate that the sound pressure responses vary with direction, with the SPLs at 0° and 45° generally higher than those in other directions. This suggests that, within this frequency band, the radiated acoustic energy is more concentrated in the forward and forward-oblique directions of the vehicle.

Further examination of the SPL curves reveals distinct peak responses at 52 Hz, 244 Hz, and 524 Hz. These peaks indicate the presence of typical structural resonances at these frequencies, which dominate the overall radiated noise characteristics. The narrowband spectral peaks at these frequencies play a decisive role in shaping the radiated acoustic signature of the vehicle.

In terms of the overall trend, the radiated source level of the small underwater vehicle exhibits relatively small fluctuations in the low-frequency range, but increases progressively with frequency, with radiated acoustic energy becoming more pronounced in the mid-to-high frequency range. This behavior is closely related to the structural stiffness of the vehicle, the characteristics of the excitation source, and the resonance properties of internal cavities. These findings provide an important basis for selecting noise-control frequency bands and optimizing target recognition frequencies in subsequent research.

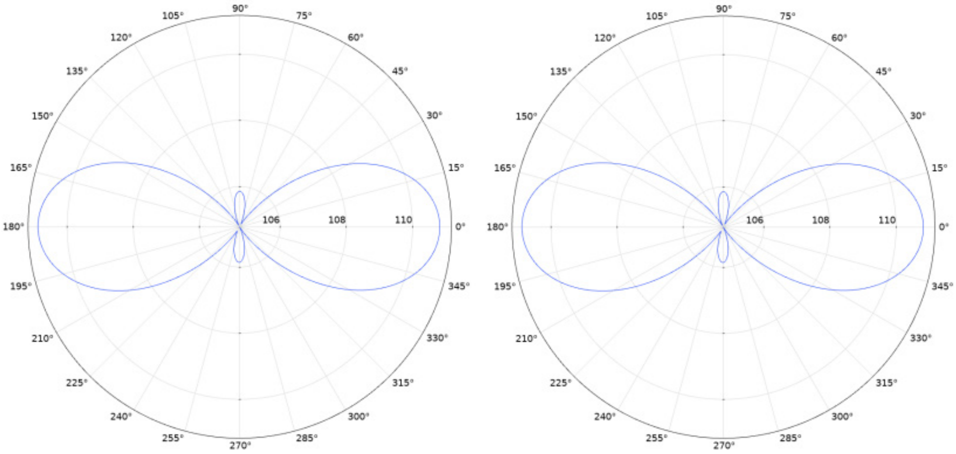

(a) Radiation Directivity Pattern at 52 Hz (b) Radiation Directivity Pattern at 244 Hz

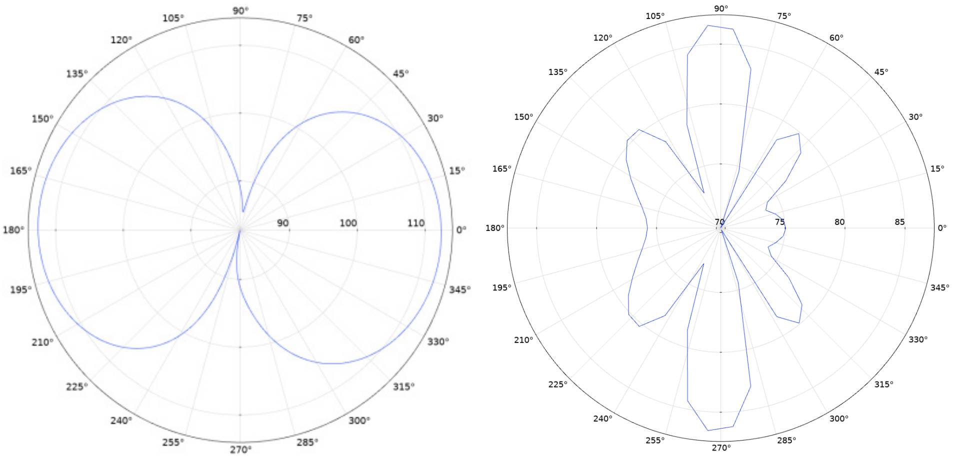

(c) HzRadiation Directivity Pattern at 524 Hz (d) Radiation Directivity Pattern at 1200 Hz

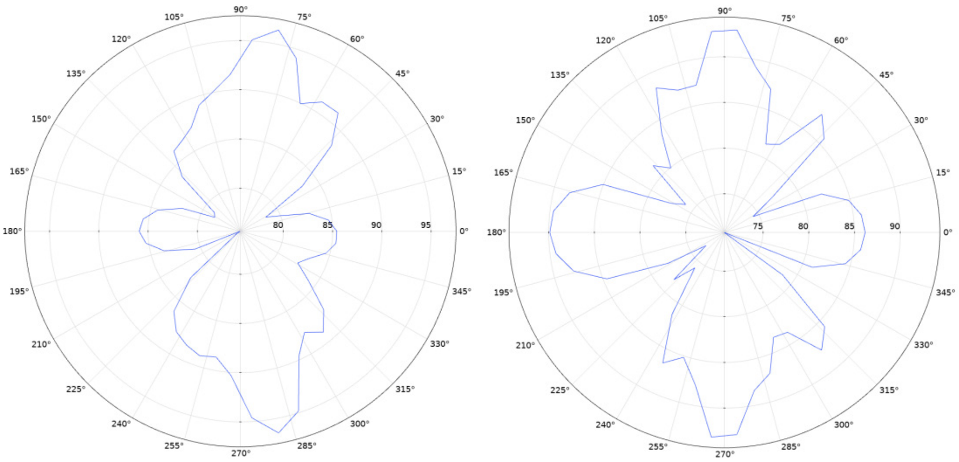

(e) Radiation Directivity Pattern at 2000 Hz (f) Radiation Directivity Pattern at 2600 Hz

Figure 8. Far-field acoustic radiation directivity of the small underwater vehicle under base excitation.

From the above figure 8, it can be observed that, after applying the excitation load, the radiated noise of the small underwater vehicle exhibits pronounced directivity characteristics. The main lobes are primarily distributed along the longitudinal axis of the structure, i.e., in the forward (0°) and aft (180°) directions, while the radiation in the lateral directions (90° and 270°) is significantly reduced, forming a distinct two-lobed far-field directivity pattern.

This characteristic indicates that, at the current calculation frequency, the radiated acoustic energy is mainly concentrated at both axial ends of the vehicle. Analysis suggests that this distribution pattern is closely related to the structural configuration of the vehicle, the location of motor-induced vibration excitations, and the propagation paths of elastic waves within the structure. In particular, when mechanical sources such as the motor are installed near the midsection, the induced structural vibrations propagate longitudinally and result in stronger radiation at the ends, thereby forming distinct main lobes in the far-field.

Although the directional sound pressure level distributions shown in the figures are not accompanied by error bars or confidence intervals, prior convergence tests on mesh density and time-step size demonstrated differences of less than 0.5 dB. This discrepancy is significantly smaller than the variations in sound radiation across different directions. Therefore, the absence of explicit uncertainty markers does not compromise the reliability of the conclusions.

Therefore, for target identification and stealth design, special attention should be given to the radiated noise characteristics at the two axial ends. Optimizing the structural layout or introducing damping measures can effectively reduce the radiated acoustic energy in these directions.

5. Conclusion

Based on the vibro-acoustic coupling simulation method, this study investigates the radiated noise characteristics of a small underwater vehicle within the frequency range of 10–3000 Hz in a typical shallow-water environment, focusing on its acoustic responses in different circumferential directions. Through the combined analysis of sound pressure level (SPL) spectra and directional comparisons, the following conclusions are drawn:

(1) Directional characteristics in the horizontal plane: The radiated noise of small underwater vehicles exhibits pronounced circumferential directivity in the horizontal plane. The far-field SPL varies with direction, with the forward (0°) radiation generally stronger than that in the lateral (90°) direction.

(2) Frequency-dependent directivity: The acoustic directivity shows significant variation with frequency. At low frequencies, structural vibrations of the stern and side hull induce localized sound pressure amplification, resulting in stronger directional characteristics. As the frequency increases, however, acoustic wave interference becomes more prominent, leading to a gradual reduction in directivity.

(3) Frequency sensitivity and amplitude fluctuations: Within the 100–3000 Hz band, the higher the frequency is, the greater the fluctuation in source level caused by changes in azimuth angle is. Multiple peak differences are observed across directions in the spectrum, indicating that the radiated response of the vehicle structure is more sensitive in the high-frequency region. This highlights the necessity of paying close attention to the influence of high-frequency features on target recognition and acoustic stealth performance.

In summary, the proposed simulation model provides a reliable characterization of the radiated noise behavior of small underwater vehicles across different frequency bands and circumferential angles. The obtained results can serve as theoretical support for target signature identification, noise control strategies, and low-observability design in practical operational scenarios.

References

[1] Zhou, C., Zhong, H., Chen, Y., et al. (2022). Review of the development of foreign diver underwater delivery platform technology. Journal of Unmanned Underwater Systems, 30(6), 680–695.

[2] Zhong, H., Han, X., & Zhou, H. (2013). A novel underwater vehicle for frogmen or payload transportation. Ship Science and Technology, 35(6), 47–51.
[3] Zhang, L. (2016). Research on measurement methods of radiated noise from propulsion motors of underwater vehicles (Master's thesis). Harbin Engineering University, China.
[4] Liu Y. M., Tang M. W., Zhou Y. J., et al. Study on the Influence of Fluid–Structure and Acoustic–Structure Coupling on the Prediction of Underwater Noise of Ships [J]. Ship Science and Technology, 2024, 46(18): 82–86.
[5] Ma, J. (2018). Study on vibro-acoustic characteristics of composite superstructures of underwater vehicles (Doctoral dissertation). Harbin Engineering University, China.
[6] Li N. Study on Acoustic Propagation Characteristics of Water-Jet Propulsor Flow Channel Based on Acoustic Finite Element Method [J]. Shipbuilding, 2023, 34(06): 50–55.
[7] STIDD Systems Inc. (2018). STIDD-DPD-System-2-CAT20-831.2-WEB-PAGES. Retrieved from http://www.stiddmil.com
[8] Dong, B. (2021). Research on underwater noise characteristics of ships in complex ocean environments (Doctoral dissertation). Harbin Engineering University, China.